Impact response of thick composite structures

NLR – Netherlands Aerospace Centre

Netherlands Aerospace Centre

NLR is a leading international research centre for aerospace. Bolstered by its multidisciplinary expertise and unrivalled research facilities, NLR provides innovative and integral solutions for the complex challenges in the aerospace sector.

NLR's activities span the full spectrum of Research Development Test & Evaluation (RDT & E). Given NLR's specialist knowledge and facilities, companies turn to NLR for validation, verification, qualification, simulation and evaluation. NLR thereby bridges the gap between research and practical applications, while working for both government and industry at home and abroad.

NLR stands for practical and innovative solutions, technical expertise and a long-term design vision. This allows NLR's cutting edge technology to find its way into successful aerospace programs of OEMs, including Airbus, Embraer and Pilatus. NLR contributes to (military) programs, such as ESA's IXV re-entry vehicle, the F-35, the Apache helicopter, and European programs, including SESAR and Clean Sky 2.

Founded in 1919, and employing some 650 people, NLR achieved a turnover of 71 million euros in 2016, of which three-quarters derived from contract research, and the remaining from government funds.

For more information visit: **www.nlr.nl**

Impact response of thick composite structures
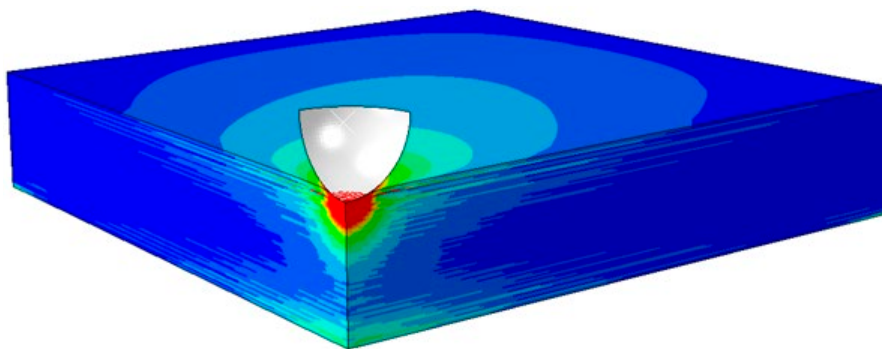
Problem area

Composite structures are known for their high specific strength properties and, unfortunately, for their low damage tolerance. Especially impact events (e.g., bird impact, hail impact, tool drops, or runway debris) are can result in significant damage which is difficult to predict. To compensate for these uncertainties, knock-down factors are used, which increase the weight and cost of the structure.

Thick composite structures (i.e., 20-50mm) are found in highly loaded aerospace structures, such as landing gear components and lugs. Their response to impact and the resulting damage can be completely different compared to thin composite structures. In addition, it is difficult to predict and quantify the damage using numerical modelling strategies.

Description of work

The goal of this report is to study the impact response of thick composite structures and identify the differences with the impact response of thin composite structures. An analytical impact response model is developed that determines the response of a thick laminate to impact in terms of force and displacement histories. A sensitivity analysis is performed that identifies the influence of impactor and laminate properties on the response. For each parameter a small-mass (i.e.,

runway debris) and large-mass (i.e., tool drop) impact case is studied. In addition a numerical model is developed and the results generally agree with the analytical model.

Results and conclusions

The results of the sensitivity analysis show the influence of several impactor and laminate properties. A small-mass impact results in a localised response where the force and plate deflection histories are out of phase, in contrast to a quasi-static response due to a large-mass impact. By increasing the impactor velocity the force and displacement increase by approximately the increase in velocity. For a large impactor radius the contact stiffness is higher, which results in a higher force and lower indentation.

A small-mass impact is not sensitive to the laminate dimensions. On the other hand, for large-mass impact the boundaries (i.e., laminate dimensions) play a significant role. Increasing the laminate thickness (or decreasing the laminate area) increases the laminate bending stiffness; as a result less energy is absorbed in bending and more in indentation.

Thicker laminates have a higher bending stiffness and therefore less impact energy transfers to bending and more is converted to indentation. Thick composite structures generally have a localised impact response which will have a significant effect on the resulting damage mechanism.

Applicability

This study is part of an on-going research program on the impact damage tolerance of thick composite structures and provides useful information for modelling the complex damage mechanisms. The next step is to develop a numerical model that can predict the impact damage in a thick composite structure. To make this model efficient the results from the analytical impact response model can be used for simplifications while keeping the same accuracy.

Impact response of thick composite structures

AUTHOR(S):

N. van Hoorn   NLR
C. Kassapoglou   Delft University of Technology
W.M. van den Brink   NLR

NLR - Netherlands Aerospace Centre

This report is based on a presentation held at the 6th ECCOMAS Thematic Conference on Mechanical Response of Composites, Eindhoven, The Netherlands, September 20-22, 2017.

The contents of this report may be cited on condition that full credit is given to NLR and the authors. This publication has been refereed by the Advisory Committee AEROSPACE VEHICLES.

CUSTOMER	**Netherlands Aerospace Centre**
CONTRACT NUMBER	**-----**
OWNER	**NLR**
DIVISION NLR	**Aerospace Vehicles**
DISTRIBUTION	**Unlimited**
CLASSIFICATION OF TITLE	**UNCLASSIFIED**

APPROVED BY :

AUTHOR	REVIEWER	MANAGING DEPARTMENT
N. van Hoorn	R.J.C. Creemers	A.A. ten Dam
DATE 0 7 1 2 1 7	DATE 0 7 1 2 1 7	DATE 1 4 1 2 1 7

Summary

Thick composite structures are used in highly loaded aerospace structures and their response to impact is not completely understood. Therefore, the goal is to study the impact response of thick composite structures and identify the differences with the impact response of thin composite structures.

Combining a Hertzian contact formulation with an analytical impact response model results in the force and displacement histories as a function of the impactor and laminate properties. Generally, the analytical impact response model agrees with numerical results. A sensitivity analysis for a small-mass and large-mass impact event shows the influence of the impactor and laminate properties on the response.

The response is especially sensitive to the impactor mass and laminate dimensions. For small-mass impact the laminate thickness significantly influences the response. On the other hand, for large-mass impact the laminate area and aspect ratio dictate the response. Thicker composite structures have a more localised response, which indicates almost no bending and more energy transfer to indentation. As a result, these structures have only internal damage in contrast to thin composite structures.

This page is intentionally left blank.

Contents

Abbreviations

ACRONYM	DESCRIPTION
CLPT	Classical Laminate Plate Theory
FSDT	First-order Shear Deformation Theory
NLR	Netherlands Aerospace Centre
ODE	Ordinary Differential Equation

1   Introduction

Fibre reinforced composite materials are increasingly being used in the aerospace industry. For instance, the new Airbus A350 and Boeing 787 both contain over 50% composites. Recently, these materials have been implemented in highly-loaded aerospace structures, such as lugs and landing gear components, resulting in thick laminates (i.e., 20-50mm or 80-200 layers). Although these composites are known for their high specific mechanical properties, their tolerance to damage is low. Impact damage (e.g., due to tool drops or runway debris) can be complex and therefore difficult to predict. To compensate for these uncertainties, conservative design strategies are used, which increases the weight and cost of the structure. Accurate damage models might be able to quantify the damage tolerance and clarify the damage mechanisms. In turn, these models could aid the design and certification process resulting in lighter and cheaper composite structures.

The laminate response to impact directly relates to the resulting damage [1]. Analytical models to predict this response are already available, for example the models of Shivakumar [2], Christoforou [3, 4], Olsson [5, 6], and more recently Talagani [7] and Esrail [8]. Their methods include energy-balance models for peak force prediction, simple spring-mass models for determining the response over time, and more complex models requiring numerical solution techniques. Despite their accurate response predictions, no studies have focused on the response of thick composite structures to impact. In addition, the difference between impact on thin and thick composite structures is unclear, including the effect of the response on the damage.

Therefore, the goal is to study the impact response of thick composite structures and identify the differences with the impact response of thin composite structures. This study is part of an on-going research program on the impact damage tolerance of thick composite structures and provides useful information for modelling the complex damage mechanisms. To obtain the elastic response, a Hertzian contact formulation is used and combined with the model of Christoforou. This model gives the force, indentation, impactor displacement, and plate deflection history depending on the laminate properties and impact characteristics (i.e., mass and velocity). These results are compared with a numerical impact response model. The sensitivity of the laminate and impact properties is analysed to determine their influence on the response, which helps to understand the impact response and identify the differences between impact on thin and thick composite structures.

2 Impact Response Prediction

This section presents an analytical and a numerical impact response model. These models predict the impact response of the laminate and impactor in terms of force and displacement. An anti-symmetric balanced transversely isotropic layup was chosen in order to comply with the assumptions in the governing equations, see below.

$$[-45,45,0,90,45,-45,90,0,0,90,45,-45,90,0,-45,45]_n$$

The number *n* defines the thickness (*h*), for example $h = 4 \cdot n$ mm if the ply thickness (t_{ply}) is 0.25mm. For this layup the B-matrix is zero, as well as the shearing-stretching coupling terms ($A_{16}=A_{26}=0$) and bending-twisting coupling terms ($D_{16} = D_{26} = 0$). The ply properties in Table 1 are assumed, which correspond to a fabric material with an 85/15 warp/weft yarn distribution. The equivalent laminate membrane properties in Table 2 are derived from the laminate stiffness tensor see appendix A. The contact stiffness and equivalent laminate membrane properties in Table 2 do not depend on the value of *n*, but the bending properties (i.e., D-matrix) increase with approximately h^3.

Table 1: Ply properties

E_{11}	110	GPa
E_{22}	25	GPa
E_{33}	7	GPa
G_{12}	5	GPa
G_{13}	5	GPa
G_{23}	4	GPa
v_{12}	0.06	-
v_{13}	0.3	-
v_{23}	0.1	-
t_{ply}	0.25	mm

Table 2: Equivalent laminate membrane properties

E_x	49.11	GPa
E_y	49.11	GPa
E_z	7.00	GPa
G_{xy}	19.05	GPa
G_{xz}	4.5	GPa
G_{yz}	4.5	GPa
v_{xy}	0.29	-
v_{xz}	0.15	-
v_{yz}	0.15	-
h	$4 \cdot n$	mm

Reference properties are established for the sensitivity analysis. A rigid spherical impactor with a radius (R_i) of 10mm is used for impact on a 200x200mm plate with a thickness of 20mm (i.e., n = 5). Two 50J impact cases are considered; a small-mass 0.04kg ($v_i = 50$m/s) impact case (e.g., runway debris), and a large-mass 4kg ($v_i = 5$m/s) impact case (e.g., tool drop).

2.1 Contact Formulation

The Hertz contact law defines the relation between the impactor indentation (δ) and contact force (*F*).

$$F = k_\alpha \delta^{3/2} \tag{1}$$

Where the indentation is the difference in impactor displacement (w_i) and centre plate deflection (w_p),

$$\delta = w_i - w_p \tag{2}$$

and the contact stiffness (k_α) is defined as,

$$k_\alpha = \frac{4E_z\sqrt{R_i}}{3(1 - v_{rz}v_{zr})} \tag{3}$$

We assume that the impactor stiffness (E_i) is significantly larger than the laminate stiffness, so that the impactor can be modelled as rigid. For a layup that is not transversely isotropic ν_{xz} is not equal to ν_{yz}. Therefore, ν_{rz} is determined by averaging the two out-of-plane Poisson's ratios. In Equation 3 the through-thickness tensile modulus (E_z) and the out-of-plane Poisson's ratios (ν_{rz} and ν_{zr}) are given in Table 2. Olsson [5] and Christoforou [4] assume that $E_z \approx E_{22}$ and that $\nu_{zr} \approx 0$ for unidirectional plies. For unidirectional plies E_{22} is approximately equal to E_{33}, in contrast to woven fabric plies. Table 1 and 2 show that $E_z = E_{33}$ and ν_{zr} can be determined to be 0.021. Olsson's and Christoforou's assumption is in line with these results considering it is a fabric material. However, E_z might be larger than E_{33} in the case the out of plane Poisson ratios (ν_{13}, ν_{23}) are higher.

The above is only accurate when the indentation is smaller than the impactor and laminate dimensions [5, 7]. However, the results in Chapter 3 show that impact on thick composite plates results in large indentation due to the lack of plate bending. Talagani concluded this also after an extensive contact study [7]. Despite this, the Hertz contact law is considered sufficient to determine elastic response.

2.2   Analytical Model

The analytical impact response model is based on Christoforou's analytical model [4]. He assumed that the plate centre deflection (w_p) is described by a series expansion.

$$w_p = \sum_{m=1}^{\infty} \sum_{n=1}^{\infty} q_{mn} s_{mn} \tag{4}$$

Here q_{mn} is the unknown amplitude and s_{mn} for centrally loaded plates is given in Equation 5. The amount of terms used (i.e., *m* and *n*) in Equation 4 defines the accuracy.

$$s_{mn} = \sin\frac{m\pi}{2}\sin\frac{n\pi}{2} \tag{5}$$

Whitney and Pagano developed plate equations of motion that include transverse shear stresses [9]. Transverse shear stresses are more dominant in thick composites, because there is almost no bending, and therefore have to be taken into account. A specially orthotropic form ($A_{16}=A_{26}=B_{ij}=D_{26}=D_{26}=0$) was derived by Dobyns, see Equation 56 [10]. Inserting Equation 4 into these plate equations of motion gives a system of second-order Ordinary Differential Equations (ODEs).

$$\frac{d^2 q_{mn}}{dt^2} + \omega_{mn}^2 q_{mn} = \frac{4F}{m_p} s_{mn} \tag{6}$$

The force is described by Equation 1 and m_p is the plate mass. The natural frequencies (ω_{mn}^2) of a simply supported composite laminate are determined using the method of Christoforou and Swanson [3], see Appendix B. In addition to a description of the plate motion, the ODE in Equation 7 describes the impactor behaviour. This equation results from substituting Equations 2 and 4 into Newton's Second Law (i.e., $m_i \ddot{w_i} = -F$).

$$\sum_{m=1}^{\infty} \sum_{n=1}^{\infty} \left(\frac{d^2 q_{mn}}{dt^2} s_{mn} \right) + \frac{d^2 \delta}{dt^2} = -\frac{F}{m_i} \tag{7}$$

Here m_i and v_i are the impactor mass and velocity. The system of *m x n + 1* second-order ODEs has to be reduced to the first order by introducing the set of variables below.

$$q_{mn,1} = q_{mn}$$

$$q_{mn,2} = q'_{mn}$$

$$\delta_1 = \delta$$

$$\delta_2 = \delta'$$

(8)

Substituting these variables and the Hertz contact law in Equations 6 and 7 gives a *2 x m x n + 2* system of first-order ODEs.

$$q'_{mn,1} = q_{mn,2}$$

$$q'_{mn,2} = \frac{4k_\alpha}{m_p} s_{mn} \delta_1^q - \omega_{mn}^2 q_{mn,1}$$

$$\delta'_1 = \delta_2$$

$$\delta'_2 = -\frac{k_\alpha}{m_i} \delta_1^q - \sum_{m=1}^{\infty} \sum_{n=1}^{\infty} s_{mn} q'_{mn,2}$$

(9)

With the corresponding initial conditions,

$$q_{mn,1}(0) = 0$$

$$q_{mn,2}(0) = 0$$

$$\delta_1(0) = 0$$

$$\delta_2(0) = v_i$$

(10)

The system of first-order ODEs described above is solved using *ode45* in *Matlab*[1]. As a result the indentation and q_{mn} are obtained as a function of time. The force history is subsequently determined using the Hertz contact law, and the plate deflection history is obtained from Equation 4. The impactor displacement history is retrieved using Equation 2, from which the impactor velocity history can be estimated.

In Figure 1, the obtained solution is compared to the results obtained by Christoforou [4]. The first peak is in perfect agreement, but there is a discrepancy in the second peak. This is probably due to small differences in the numerical solution procedure and the determination of the plate natural frequencies. Despite this, the result in Figure 1 verifies the method because only the first peak is of interest for this study.

Talagani compared his solution with 5J impact experiments on a thin composite plate performed by Lopes [11, 7]. The results of the current implementation of Christoforou's model are added in Figure 2. This validation is limited because it considers a low-energy impact on a thin laminate, which is outside the scope of this study. Beside a shift in the plate oscillations, the results agree with the experimental results of Lopes, and are in line with Talagani's model.

---

[1] *ode45* solves non-stiff differential equations based on a variable step Runge-Kutta method.
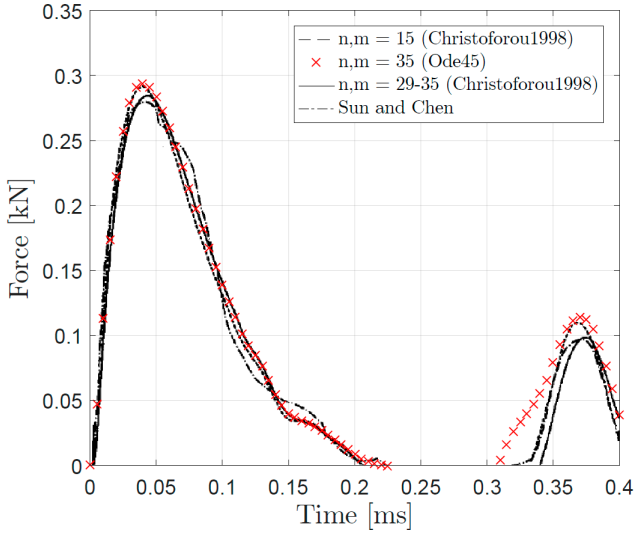
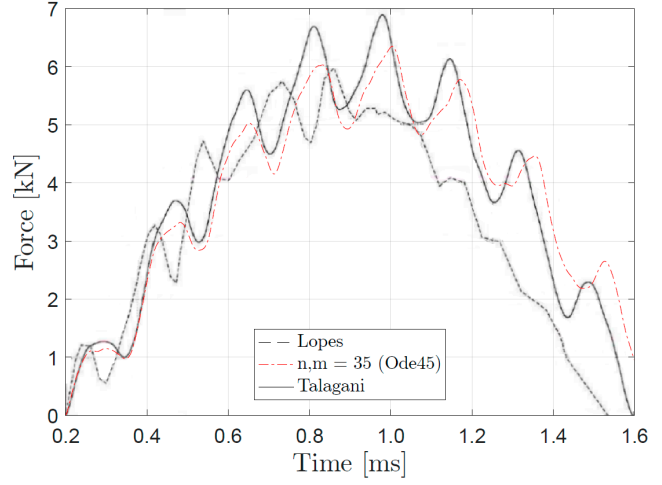Figure 1: Comparison of the analytical impact response model solution and Christoforou's solution [4].

Figure 2: Comparison of the analytical impact response model solution and experiments performed by Lopes [11, 7].

Flexural waves significantly affect the response in certain cases. These waves travel a certain distance within the impact duration (t_{imp}). This impact duration, or end of impact, is defined as the moment when the impactor displacement is zero again. The area affected by these travelling flexural waves (i.e., wave affected area) can be determined from the wave front of the first mode. Equation 11 describes this area in terms of an ellipse with $r(\theta)$ [6, 12]. $D_r(0°) = D_{11}$ and $D_r(90°) = D_{22}$ which are the only two values required to define the wave affected area in terms of an ellipse.

$$r(\theta) = \sqrt{\pi t_{imp}} \left[\frac{D_r(\theta)}{h\rho} \left(\frac{D_{12} + 2D_{33}}{\sqrt{D_{11}D_{22}}} + 1 \right) \right]^{1/4} \tag{11}$$

2.3   Numerical Model

To compare the analytical impact response model to numerical results we developed a numerical model in ABAQUS/Explicit. The impact times are short (e.g., 0.1ms for small-mass impact and 1ms for large-mass impact), which makes an explicit solver suitable. As will become clear, different modelling strategies result in a trade-off between computational time and accuracy.

The most expensive and accurate model is a layer-by-layer model with continuum solid elements (C3D8R). For this model, the ply properties in Table 1 and the corresponding orientations are assigned to each ply. Hard frictionless contact describes the interaction between the impactor and laminate. The model employs quarter symmetry, which has a small effect on the response in terms of force and displacement. However, using quarter symmetry affects the internal stress distribution because $E_{11} \neq E_{22}$, which will give inaccurate damage predictions.
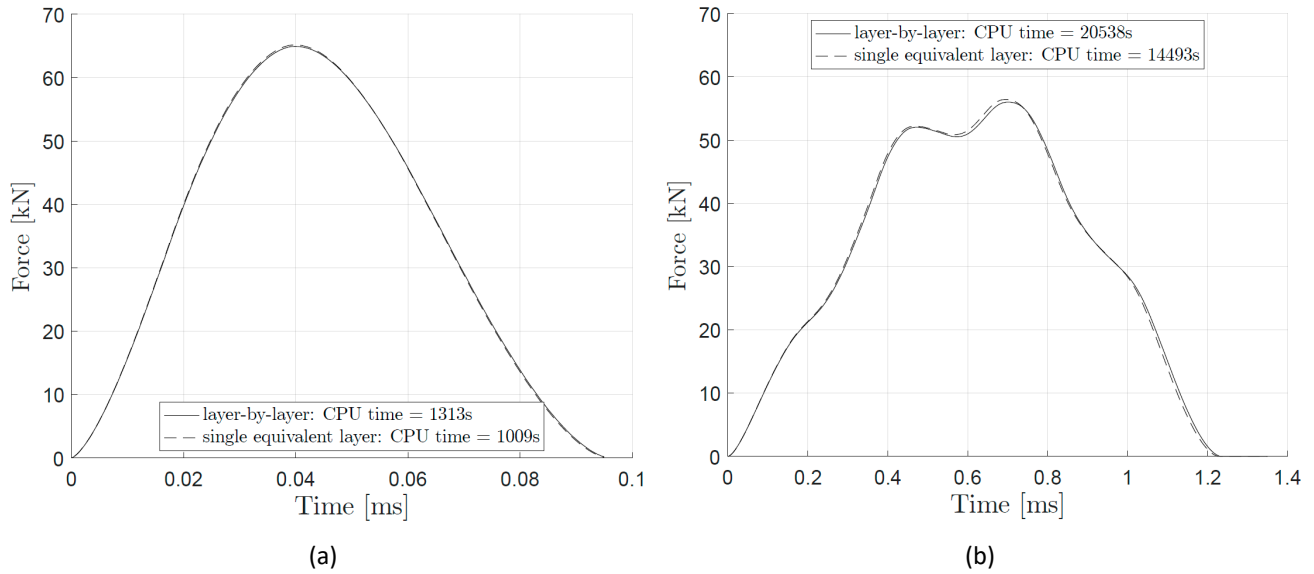
Figure 3: Comparison of the layer-by-layer and single equivalent layer numerical impact response model for (a) small-mass and (b) large-mass impact.

To reduce computational time one can model the laminate as a single equivalent layer with the laminate properties given in Table 2. Both models give almost identical results beside a negligible (e.g. 0.15%) increase in peak force for the equivalent single layer model, see Figure 3. The computational time of the equivalent single layer model is on average 25% lower compared to the layer-by-layer model. An additional advantage is that the mesh density can be decreased.

Several meshing strategies are investigated, where the mesh density is expressed in terms of elements through the thickness (n_t). A uniform mesh with $n_t = 80$ (i.e., one element per ply) is computationally expensive. One option is to decrease mesh density towards the plate edges, so that a locally refined region remains at the impact location. Compared to the uniform mesh the response is identical while the computational time decreased by 94%. In addition, the results converge for $n_t = 40$ (i.e., 0.5mm) and result in an additional 84% decrease in computational time compared to $n_t = 80$. At last, the dimensions of the locally refined region are increased and the results converge at 3x3mm.

Beside C3D8R elements the continuum shell element (SC8R) is commonly used. This element has a shell like response but a continuum topology. The simulations show that the SC8R elements have problems with the localised indentation due to a limited through-thickness description compared to the C3D8R elements. Moreover, the SC8R elements cause a 40% increase in computational time. SC8R elements are not suitable for localised impact cases where large indentations are involved.

3   Results and Observations

Section 3.1 compares the numerical and analytical model. This comparison is arbitrary because ideally both models should be compared to experimental data. However, Figure 2 shows that the analytical model is reasonably close to experimental results. Because both the analytical and numerical models assume that no damage occurs, it makes sense to compare these models. In addition to the analytical model based on Christoforou, the comparison includes the small-mass impact model of Olsson [5] and the energy-balance model of Esrail [8].

3.1   Comparison of Impact Response Models

Figure 3(a) compares the impact response models for the small-mass impact event. The response shape of all models is similar, but the peak force and impact duration differ. In contrast to Christoforou's model, Olsson's model uses the *Classical Laminated Plate Theory* (CLPT) to determine the plate natural frequencies. If the transverse shear stresses are included in Olsson's model (i.e., by using Equation 57) the results are identical to Christoforou's model. Christoforou's model predicts a lower peak force compared to the numerical model, which is also seen for the large-mass impact event in Figure 4(b). The difference results from a factor 2.2 lower contact stiffness in the analytical model compared to 'hard contact' in the numerical model. Nevertheless, the analytical model agrees with experimental results (see Figure 2) and the correct response shape is predicted. Olsson's model is based on a single mass spring, and is therefore not able to capture the large-mass quasi-static response.

(a)   (b)
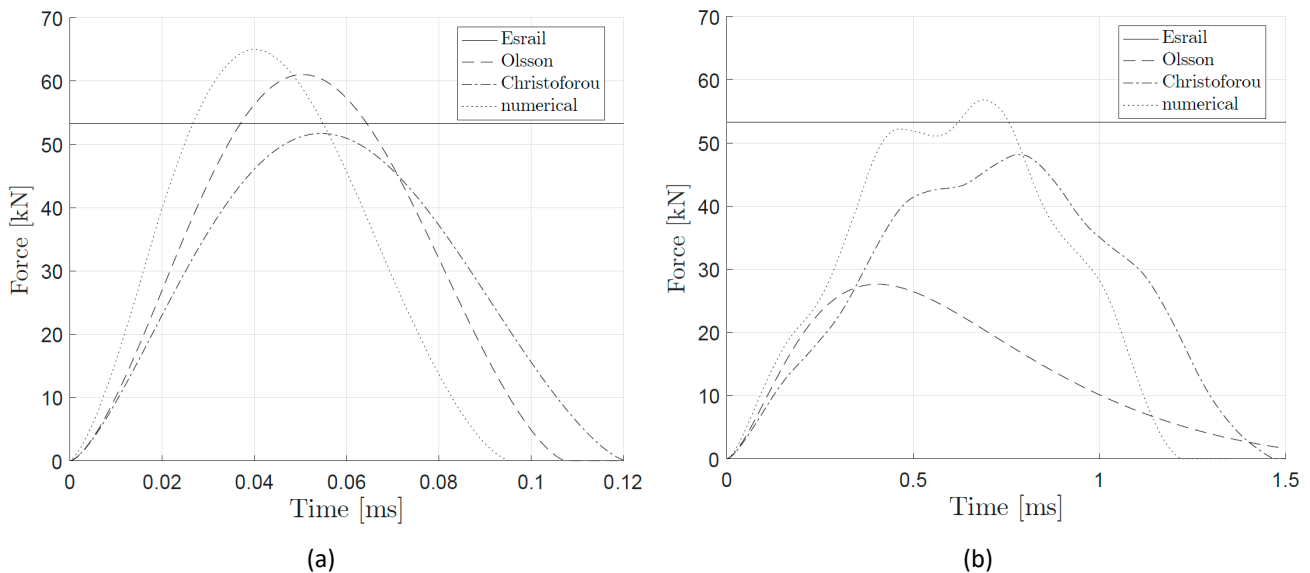
Figure 4: Comparison of the analytical impact response model (Christoforou), Olsson's small-mass impact response model, Esrail's energy-balance model, and the numerical impact response model for (a) small-mass and (b) large-mass impact. For small-mass impact, Christoforou's and Olsson's model give identical results, but Olsson's model is not able to capture the response for large-mass impact. The numerical model is in line with Christoforou's model and the peak force prediction of Esrail.

3.2 Sensitivity Analysis

In this section, a sensitivity analysis determines the sensitivity of the impact and laminate parameters using the analytical impact response model. Each case evaluates a small-mass and large-mass impact event, except for the impactor mass sensitivity. The parameters that determine the response are varied independently compared to the reference properties in bold.

- Impactor mass (m_i): **0.04** - 0.4 - **4** kg (constant E_i)
- Impactor energy (E_i): **50** - 128 - 200 J (constant m_i)
- Impactor radius (R_i): 5 - **10** - 20 mm
- Laminate thickness (h): 12 - **20** - 40 mm
- Laminate area (a,b): 100 - **200** - 400 mm
- Laminate aspect ratio (AR): **1** - 2 - 4 (constant area)

The sensitivity to the impactor mass is high and it can significantly change the impact response. For instance, the impact duration increases from approximately 0.12 to 0.50 and to 1.47ms. Figure 5 shows the difference between the three types of impact (i.e., small-mass, intermediate-mass, and large-mass impact) by plotting the force and plate deflection versus normalised time. In contrast to a large-mass impact, the force and plate deflection are out of phase for a small-mass impact. For the intermediate-mass impact, the force and plate deflection are also out of phase. In addition, the force history is complex, as it can increase and decrease significantly over time, simulating multiple impacts (see Figure 7(b)).
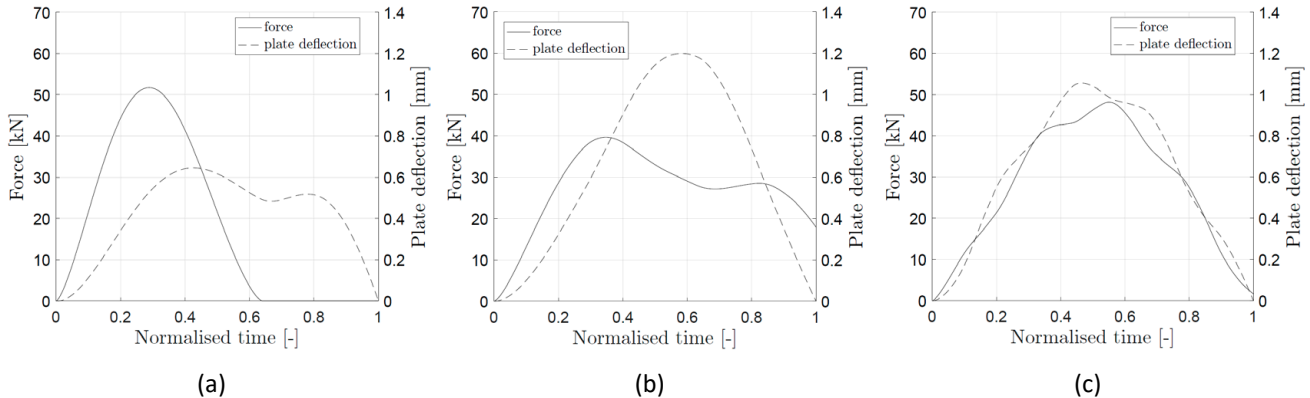

(a) (b) (c)

Figure 5: Force and plate deflection histories illustrating the impactor mass sensitivity for (a) small-mass, (b) intermediate-mass, and (c) large-mass impact. In contrast to large-mass impact, the force and plate deflection are out of phase for small-mass impact.

The transition between the response types also involves the wave affected area as discussed in Section 2.2 and determined by Equation 11. For the reference plate, it takes 0.066ms for the flexural (i.e., bending) waves to reach the boundaries of the specimen. At 0.132ms (i.e., 2x0.066ms) the flexural waves are back at the impact location and the plate oscillations start to affect the response. However, for small-mass impact the event is already over, and thus these oscillations have no influence on the response. On the other hand, the plate oscillations are visible in Figure 5(c) but the impact duration (i.e., 1.47ms) is too long to significantly affect the response. For some intermediate-mass impacts, the plate oscillations can significantly affect the response.
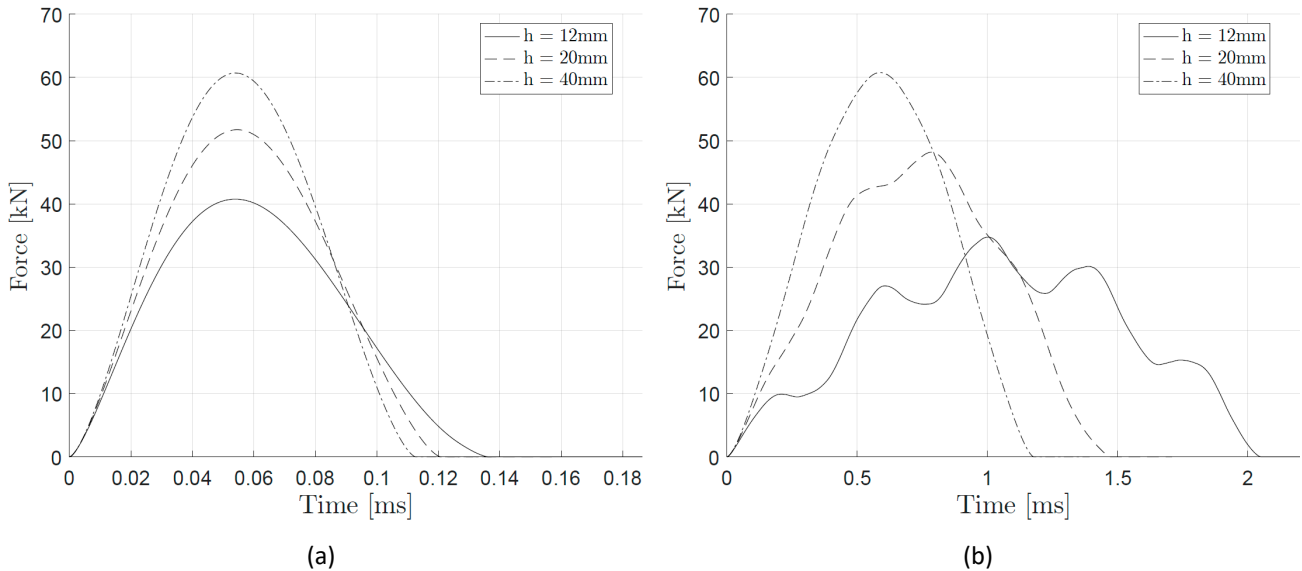
Figure 6: Force histories illustrating the laminate thickness sensitivity for (a) small-mass and (b) large-mass impact.

For a constant impactor mass, the response sensitivity to the impactor energy is low. However, the force and displacements are increased with approximately the impactor velocity while the impact duration is only slightly decreased. This is expected, as the velocity is only an initial condition and can be seen as the amplitude of the system of differential equations. Similarly, the sensitivity to the impactor radius has no significant effect on the response shape, but increasing the impactor radius increases the force and decreases the impactor displacement. This effect is identical to scaling the contact stiffness (k_α).

The laminate dimensions have a high sensitivity, for instance the thickness (Figure 6), the area (Figure 7), and the aspect ratio (Figure 8). Increasing the thickness as well as the area doubles the laminate mass and according to Olsson the impactor/plate mass ratio dictates the response [6]. Olsson stated that a ratio below 0.23 can be considered small-mass and above 2.0 large-mass impact. However, the results show that the sensitivity to these parameters is different. This indicates that the laminate bending stiffness also plays a significant role. For example, increasing the thickness or decreasing the area results in a higher bending stiffness. Overall, the area within the force-displacement curve decreases for an increasing thickness. For thicker laminates, more energy is absorbed into indentation during the loading phase, instead of bending energy. For example, according to the model of Esrail [8], for a thickness of 12mm about 88% of the energy converts to bending energy compared to 17% for a 40mm thick laminate. For small-mass impact not all energy is transferred back to kinetic energy. However, increasing the laminate thickness results in a residual velocity closer to the initial velocity. For large-mass impact, all energy is converted back to kinetic energy resulting in a residual velocity equal to the initial velocity.
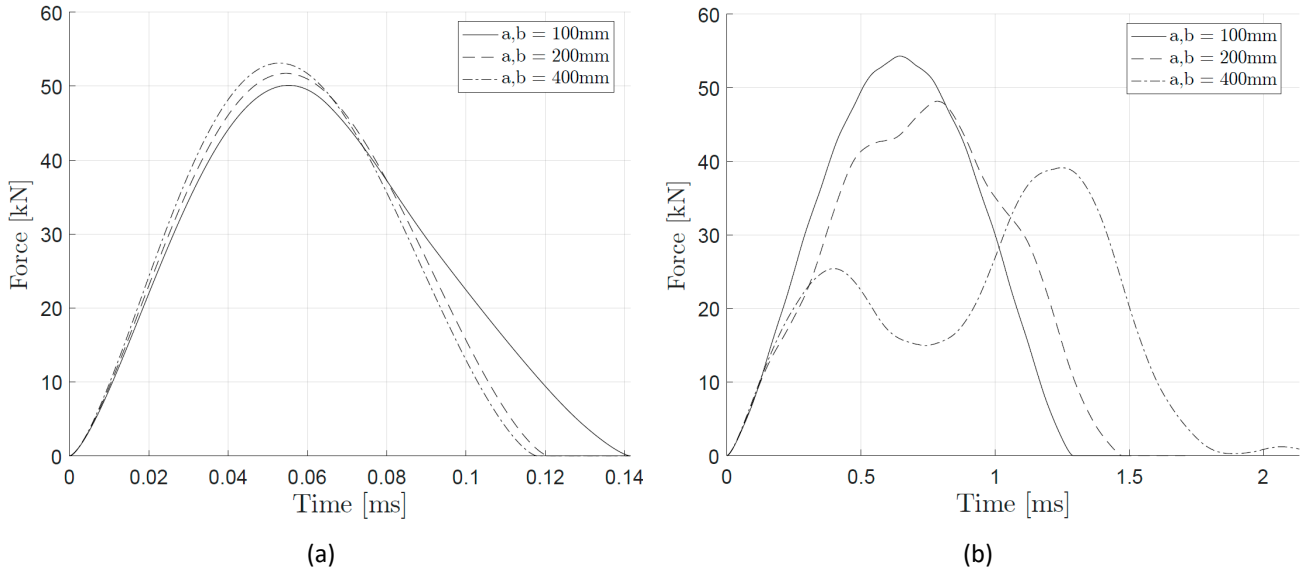
Figure 7: Force history illustrating the laminate area sensitivity for (a) small-mass and (b) large-mass impact.

In contrast to large-mass impact, increasing the laminate area above 200x200mm has almost no effect on the response for small-mass impact (see Figure 7). Figure 8 shows the sensitivity to the laminate aspect ratio. For large-mass impact the sensitivity is low compared to Figure 7(b). However, for small-mass impact a higher aspect ratio results in a significant higher force. The results in this section show that there are many parameters that affect the response. In contrast to a localised small-mass impact, the laminate dimensions and boundary conditions significantly influence the large-mass impact response, which agrees with Olsson's conclusions [6].
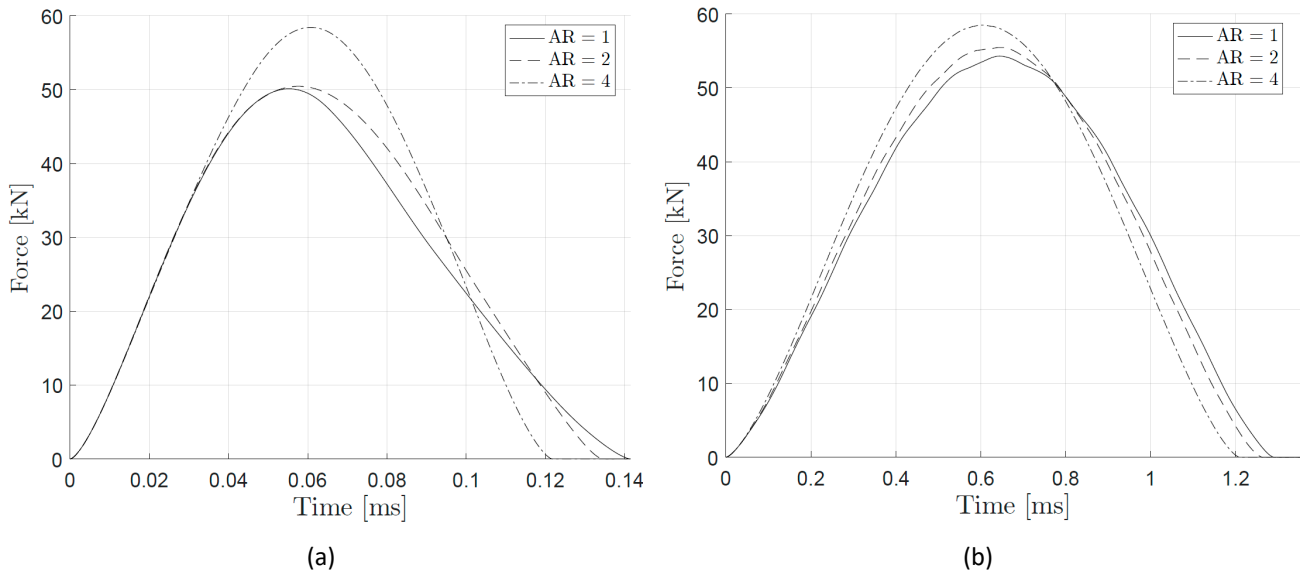

Figure 8: Force history illustrating the laminate aspect ratio sensitivity for (a) small-mass and (b) large-mass impact.

4   Conclusions and Future Work

This paper has studied the impact response of thick composite structures and identified the differences with the impact response of thin composite structures. An analytical impact response model was developed, based on the methodology of Christoforou [4], which includes the Hertz contact law. The results were compared with a numerical impact response model and overall the response of both models agreed. A sensitivity analysis on several key parameters was performed using the analytical impact response model. Two 50J impact cases, a small-mass (0.04kg) and a large-mass (4kg), were studied. The sensitivity analysis lead to the following conclusions:

- For small-mass impact, the force and plate deflection histories are out of phase (i.e., localised response).
- On the other hand, a large-mass impact has a quasi-static response where these histories align.
- A complex response, with multiple impact events, can occur for impactor masses between small-mass and large-mass (i.e., intermediate-mass).
- Increasing the impactor velocity, while keeping the impactor mass constant, scales the force and displacement by approximately the increase in velocity.
- For a large impactor radius, the contact stiffness is higher, which results in a higher force and lower indentation.
- Beside the increase in peak force for thicker laminates, a small-mass impact is not sensitive to the laminate dimensions.
- For large-mass impact, the laminate dimensions play a significant role.
    - o A thicker laminate has a higher laminate bending stiffness. As a result, the impact energy is mainly converted to indentation instead of bending. The peak force is therefore significantly higher for thicker laminates, while the impact duration is shorter.
    - o Decreasing the area gives similar results as increasing the thickness.
    - o A higher aspect ratio (constant area) increases the peak force, but the impact duration decreases.

The response of thick composite structures to impact can be completely different from the response of thin composite structures. In the end, the energy that goes into bending and indentation will result in damage. Thick composite structures generally have a localised impact response, whereas thin composite structures tend towards a quasi-static impact response with more bending. The difference in response will have a significant effect on the resulting damage mechanism. According to literature and previous studies a local response results in mostly internal damage (e.g., matrix cracking and delaminations) and maybe a dent at the impact location. A quasi-static response can result in external damage in the form of fibre breakage. The results of this paper give valuable information about the effect of impactor and laminate characteristics on the resulting response. The next step is to use this information to predict the extent and type of damage with a numerical model. This model can aid the design and certification process of thick composite structures, which can result in lighter aerospace components.

5   References

1.   G. A. O. Davies and R. Olsson. Impact on composite structures. *The Aeronautical Journal*, 108:541–563, November 2004.

2.   K.N. Shivakumar, W. Elber, and W. Illg. Prediction of impact force and duration due to low-velocity impact on circular composite laminates. *Journal of Applied Mechanics*, 52(3):674–680, September 1985.

3.   A.P. Christoforou and S.R. Swanson. Analysis of impact response in composite plates. *International Journal of Solids and Structures*, 27(2):161–170, 1991.

4.   A.P. Christoforou and A.S. Yigit. Characterization of impact in composite plates. *Composite Structures*, 43:14–24, 1998.

5.   R. Olsson. Impact response of orthotropic composite plates predicted from a one-parameter differential equation. *AIAA Journal*, 30(6):1587–1596, June 1992.

6.   R. Olsson. Mass criterion for wave controlled impact response of composite plates. *Composites Part A: Applied Science and Manufacturing*, 31(8):879–887, August 2000.

7.   M.R. Talagani. *Impact analysis of composite structures*. Phd thesis, Delft University of Technology, December 2014.

8.   F. Esrail and C. Kassapoglou. An efficient approach for damage quantification in quasi-isotropic composite laminates under low speed impact. *Composites Part B: Engineering*, 61:116–126, May 2014.

9.   J. M. Whitney and N. J. Pagano. Shear deformation in heterogeneous anisotropic plates. *Journal of Applied Mechanics*, 37(4):1031–1036, December 1970.

10.   A. L. Dobyns. Analysis of simply-supported orthotropic plates subject to static and dynamic loads. *AIAA Journal*, 19(5):642–650, May 1981.

11.   C.S. Lopes. *Damage and Failure of Non-Conventional Composite Laminates*. Phd thesis, Delft University of Technology, June 2009.

12.   R.J.C. Creemers. Effect of impact damage and subsequent fatigue loading on thick composite structures: test results - vol 1. techreport NLR-CR-2011-437-VOL-1, NLR -Netherlands Aerospace Centre, 2011.

13.   C. Kassapoglou. *Design and analysis of composite structures*. John Wiley & Sons, Ltd, 2010.

Appendix A Derivation of the Equivalent Laminate Membrane Properties

The compliance tensor that relates the stresses to the strains, for an orthotropic laminate can be defined [13].

$$\begin{Bmatrix} \varepsilon_x \\ \varepsilon_y \\ \varepsilon_z \\ \gamma_{yz} \\ \gamma_{xz} \\ \gamma_{xy} \end{Bmatrix} = \begin{bmatrix} S_{11} & S_{12} & S_{13} & 0 & 0 & S_{16} \\ S_{12} & S_{22} & S_{23} & 0 & 0 & S_{26} \\ S_{13} & S_{23} & S_{33} & 0 & 0 & S_{36} \\ 0 & 0 & 0 & S_{44} & S_{45} & 0 \\ 0 & 0 & 0 & S_{45} & S_{55} & 0 \\ S_{16} & S_{26} & S_{36} & 0 & 0 & S_{66} \end{bmatrix} \begin{Bmatrix} \sigma_x \\ \sigma_y \\ \sigma_z \\ \tau_{yz} \\ \tau_{xz} \\ \tau_{xy} \end{Bmatrix} \tag{12}$$

For each ply k that is at an angle θ the values for S_{ij}^k can be determined by transforming the ply properties to the laminate coordinate system.

$$S_{11}^k = \frac{1}{E_{11}} cos^4\theta + \left(\frac{1}{G_{12}} - \frac{2\nu_{12}}{E_{11}} \right) sin^2\theta \, cos^2\theta + \frac{1}{E_{22}} sin^4\theta \tag{13}$$

$$S_{12}^k = \left(\frac{1}{E_{11}} + \frac{1}{E_{22}} - \frac{1}{G_{12}} \right) sin^2\theta \, cos^2\theta - \frac{\nu_{12}}{E_{11}} (sin^4\theta + cos^4\theta) \tag{14}$$

$$S_{13}^k = -\frac{\nu_{13}}{E_{11}} cos^2\theta - \frac{\nu_{23}}{E_{22}} sin^2\theta \tag{15}$$

$$S_{22}^k = \frac{1}{E_{11}} sin^4\theta + \left(\frac{1}{G_{12}} - \frac{2\nu_{12}}{E_{11}} \right) sin^2\theta \, cos^2\theta + \frac{1}{E_{22}} cos^4\theta \tag{16}$$

$$S_{23}^k = -\frac{\nu_{13}}{E_{11}} sin^2\theta - \frac{\nu_{23}}{E_{22}} cos^2\theta \tag{17}$$

$$S_{33}^k = \frac{1}{E_{33}} \tag{18}$$

$$S_{16}^k = \frac{2}{E_{11}} cos^3\theta \, sin\theta - \frac{2}{E_{22}} cos\theta \, sin^3\theta + \left(\frac{1}{G_{12}} - \frac{2\nu_{12}}{E_{11}} \right) (cos\theta \, sin^3\theta - cos^3\theta \, sin\theta) \tag{19}$$

$$S_{26}^k = \frac{2}{E_{11}} cos\theta \, sin^3\theta - \frac{2}{E_{22}} cos^3\theta \, sin\theta + \left(\frac{1}{G_{12}} - \frac{2\nu_{12}}{E_{11}} \right) (cos^3\theta \, sin\theta - cos\theta \, sin^3\theta) \tag{20}$$

$$S_{36}^k = 2 \left(\frac{\nu_{23}}{E_{22}} - \frac{\nu_{13}}{E_{11}} \right) cos\theta \, sin\theta \tag{21}$$

$$S_{44}^k = \frac{1}{G_{13}} sin^2\theta + \frac{1}{G_{23}} cos^2\theta \tag{22}$$

$$S_{45}^k = \left(\frac{1}{G_{13}} - \frac{1}{G_{23}} \right) sin\theta \, cos\theta \tag{23}$$

$$S_{55}^k = \frac{1}{G_{13}} cos^2\theta + \frac{1}{G_{23}} sin^2\theta \tag{24}$$

$$S_{66}^k = 4\left(\frac{1}{E_{11}} + \frac{1}{E_{22}} + \frac{2v_{12}}{E_{11}}\right)\sin^2\theta\cos^2\theta + \frac{1}{G_{12}}(\sin^4\theta + \cos^4\theta - 2\sin^2\theta\cos^2\theta) \tag{25}$$

The inverse of the ply compliance tensor gives the ply stiffness tensor, for instance $\boldsymbol{C} = (\boldsymbol{S})^{-1}$. With the equal strain assumption, the laminate stiffness tensor can be obtained by averaging the components,

$$C_{ij} = \frac{1}{h}\sum_{k=1}^{n} C_{ij}^k\, t_k \tag{26}$$

where t_k is the thickness of ply k and h the laminate thickness.

$$\begin{Bmatrix} \sigma_x \\ \sigma_y \\ \sigma_z \\ \tau_{yz} \\ \tau_{xz} \\ \tau_{xy} \end{Bmatrix} = \begin{bmatrix} C_{11} & C_{12} & C_{13} & 0 & 0 & C_{16} \\ C_{12} & C_{22} & C_{23} & 0 & 0 & C_{26} \\ C_{13} & C_{23} & C_{33} & 0 & 0 & C_{36} \\ 0 & 0 & 0 & C_{44} & C_{45} & 0 \\ 0 & 0 & 0 & C_{45} & C_{55} & 0 \\ C_{16} & C_{26} & C_{36} & 0 & 0 & C_{66} \end{bmatrix} \begin{Bmatrix} \varepsilon_x \\ \varepsilon_y \\ \varepsilon_z \\ \gamma_{yz} \\ \gamma_{xz} \\ \gamma_{xy} \end{Bmatrix} \tag{27}$$

From the compliance tensor of the full laminate above the equivalent laminate properties (i.e., E_x, E_y, E_z) can be determined. For example, to determine E_x one can assume a uniaxial tension test such that $\sigma_x \neq 0$ and $\sigma_y = \sigma_z = \tau_{yz} = \tau_{xz} = \tau_{xy} = 0$. The system of equations as in Equation 27 can then be rewritten,

$$C_{11}\varepsilon_x + C_{12}\varepsilon_y + C_{13}\varepsilon_z + C_{16}\gamma_{xy} = \sigma_x \tag{28}$$

$$C_{12}\varepsilon_x + C_{22}\varepsilon_y + C_{23}\varepsilon_z + C_{26}\gamma_{xy} = 0 \tag{29}$$

$$C_{13}\varepsilon_x + C_{23}\varepsilon_y + C_{33}\varepsilon_z + C_{36}\gamma_{xy} = 0 \tag{30}$$

$$C_{16}\varepsilon_x + C_{26}\varepsilon_y + C_{36}\varepsilon_z + C_{66}\gamma_{xy} = 0 \tag{31}$$

Rearranging Equations 29 - 31 gives,

$$\varepsilon_y = \frac{-C_{12}\varepsilon_x - C_{23}\varepsilon_z - C_{26}\gamma_{xy}}{C_{22}} \tag{32}$$

$$\varepsilon_z = \frac{-C_{13}\varepsilon_x - C_{23}\varepsilon_y - C_{36}\gamma_{xy}}{C_{33}} \tag{33}$$

$$\gamma_{xy} = \frac{-C_{16}\varepsilon_x - C_{26}\varepsilon_y - C_{36}\varepsilon_z}{C_{66}} \tag{34}$$

Inserting Equation 32 in Equation 33, regrouping, and simplifying gives,

$$\varepsilon_z = -v_{xz}\varepsilon_x \tag{35}$$

where,

$$v_{xz} = \frac{C_{13}C_{26}^2 - C_{16}C_{23}C_{26} - C_{12}C_{26}C_{36} + C_{16}C_{22}C_{36} + C_{12}C_{23}C_{66} - C_{13}C_{22}C_{66}}{C_{66}C_{23}^2 - 2C_{23}C_{26}C_{36} + C_{33}C_{26}^2 + C_{22}C_{36}^2 - C_{22}C_{33}C_{66}} \tag{36}$$

The same can be done by inserting Equation 33 in Equation 32,

$$\varepsilon_y = -v_{xy}\varepsilon_x \tag{37}$$

where,

$$\nu_{xy} = \frac{C_{12}C_{36}^2 - C_{13}C_{26}C_{36} - C_{16}C_{23}C_{36} + C_{16}C_{26}C_{33} + C_{13}C_{23}C_{66} - C_{12}C_{33}C_{66}}{C_{66}C_{23}^2 - 2C_{23}C_{26}C_{36} + C_{33}C_{26}^2 + C_{22}C_{36}^2 - C_{22}C_{33}C_{66}} \tag{38}$$

Substituting Equations 35 and 37 into Equation 34 gives,

$$\gamma_{xy} = \frac{-C_{12} + C_{26}\nu_{xy} + C_{36}\nu_{xz}}{C_{66}}\varepsilon_x \tag{39}$$

Finally, insert Equations 35, 37, and 40 back into Equation 28 to give the expression for E_x,

$$\sigma_x = E_x \varepsilon_x \tag{40}$$

where,

$$E_x = C_{11} - \nu_{xy}\left(C_{12} - \frac{C_{16}C_{26}}{C_{66}}\right) - \nu_{xz}\left(C_{13} - \frac{C_{16}C_{36}}{C_{66}}\right) - \frac{C_{16}^2}{C_{66}} \tag{41}$$

In a similar fashion E_y and E_z and the corresponding Poisson ratios can be derived,

$$E_y = C_{22} - \nu_{yz}\left(C_{12} - \frac{C_{16}C_{26}}{C_{66}}\right) - \nu_{yz}\left(C_{23} - \frac{C_{26}C_{36}}{C_{66}}\right) - \frac{C_{26}^2}{C_{66}} \tag{42}$$

$$\nu_{yz} = \frac{C_{16}^2C_{23} - C_{13}C_{16}C_{26} - C_{12}C_{16}C_{36} + C_{11}C_{26}C_{36} + C_{12}C_{13}C_{66} - C_{11}C_{23}C_{66}}{C_{66}C_{13}^2 - 2C_{13}C_{16}C_{36} + C_{33}C_{16}^2 + C_{11}C_{36}^2 - C_{11}C_{33}C_{66}} \tag{43}$$

$$\nu_{yx} = \frac{C_{12}C_{36}^2 - C_{13}C_{26}C_{36} - C_{16}C_{23}C_{36} + C_{16}C_{26}C_{33} + C_{13}C_{23}C_{66} - C_{12}C_{33}C_{66}}{C_{66}C_{13}^2 - 2C_{13}C_{16}C_{36} + C_{33}C_{16}^2 + C_{11}C_{36}^2 - C_{11}C_{33}C_{66}} \tag{44}$$

$$E_z = C_{33} - \nu_{zx}\left(C_{13} - \frac{C_{16}C_{36}}{C_{66}}\right) - \nu_{zy}\left(C_{23} - \frac{C_{26}C_{36}}{C_{66}}\right) - \frac{C_{36}^2}{C_{66}} \tag{45}$$

$$\nu_{zy} = \frac{C_{16}^2C_{23} - C_{13}C_{16}C_{26} - C_{12}C_{16}C_{36} + C_{11}C_{26}C_{36} + C_{12}C_{13}C_{66} - C_{11}C_{23}C_{66}}{C_{66}C_{12}^2 - 2C_{12}C_{16}C_{26} + C_{22}C_{16}^2 + C_{11}C_{26}^2 - C_{11}C_{22}C_{66}} \tag{46}$$

$$\nu_{zx} = \frac{C_{13}C_{26}^2 - C_{16}C_{23}C_{26} - C_{12}C_{26}C_{36} + C_{16}C_{22}C_{36} + C_{12}C_{23}C_{66} - C_{13}C_{22}C_{66}}{C_{66}C_{12}^2 - 2C_{12}C_{16}C_{26} + C_{22}C_{16}^2 + C_{11}C_{26}^2 - C_{11}C_{22}C_{66}} \tag{47}$$

For determining G_{yz} one can assume that $\tau_{yz} \neq 0$ and $\sigma_x = \sigma_y = \sigma_z = \tau_{xz} = \tau_{xy} = 0$. The system of equations as in Equation 27 can then be rewritten,

$$C_{44}\gamma_{yz} + C_{45}\gamma_{xz} = \tau_{yz} \tag{48}$$

$$C_{45}\gamma_{yz} + C_{55}\gamma_{xz} = 0 \tag{49}$$

Because the resulting equations do not depend on many variables, the derivation is quite straightforward. Rewriting Equation 49 and substituting in Equation 48 gives,

$$\tau_{yz} = G_{yz}\gamma_{yz} \tag{50}$$

where,

$$G_{yz} = C_{44} - \frac{C_{45}^2}{C_{55}}$$

(51)

Similarly for G_{xz} this gives,

$$G_{xz} = C_{55} - \frac{C_{45}^2}{C_{44}}$$

(52)

The derivation of G_{xy} can be done similarly to the derivation of E_x which will result in,

$$G_{xy} = C_{66} - v_{xyy}(C_{26} - \frac{C_{12}C_{16}}{C_{11}}) - v_{xyz}(C_{36} - \frac{C_{13}C_{16}}{C_{11}}) - \frac{C_{16}^2}{C_{11}}$$

(53)

where,

$$v_{xyz} = \frac{C_{12}^2 C_{36} - C_{12}C_{13}C_{26} - C_{12}C_{16}C_{23} + C_{13}C_{16}C_{22} + C_{11}C_{23}C_{26} - C_{11}C_{22}C_{36}}{C_{33}C_{12}^2 - 2C_{12}C_{13}C_{23} + C_{22}C_{13}^2 + C_{11}C_{23}^2 - C_{11}C_{22}C_{33}}$$

(54)

$$v_{xyy} = \frac{C_{13}^2 C_{26} - C_{13}C_{16}C_{23} - C_{12}C_{13}C_{36} + C_{12}C_{16}C_{33} + C_{11}C_{23}C_{36} - C_{11}C_{26}C_{33}}{C_{33}C_{12}^2 - 2C_{12}C_{13}C_{23} + C_{22}C_{13}^2 + C_{11}C_{23}^2 - C_{11}C_{22}C_{33}}$$

(55)

Appendix B Derivation of the Plate Natural Frequencies

The plate equations of motions for a specially orthotropic plate are given below [10].

$$D_{11} \frac{\partial^2 \Psi_x}{\partial x^2} + D_{66} \frac{\partial^2 \Psi_x}{\partial y^2} + (D_{12} + D_{66}) \frac{\partial^2 \Psi_y}{\partial x \, \partial y} - kA_{55} \left(\Psi_x + \frac{\partial w}{\partial x} \right) = \frac{\rho h^3}{12} \frac{\partial^2 \Psi_x}{\partial t^2}$$

$$(D_{12} + D_{66}) \frac{\partial^2 \Psi_y}{\partial x \, \partial y} + D_{66} \frac{\partial^2 \Psi_y}{\partial x^2} + D_{22} \frac{\partial^2 \Psi_y}{\partial y^2} - kA_{44} \left(\Psi_y + \frac{\partial w}{\partial x} \right) = \frac{\rho h^3}{12} \frac{\partial^2 \Psi_y}{\partial t^2}$$

$$kA_{55} \left(\frac{\partial \Psi_x}{\partial x} + \frac{\partial^2 w}{\partial x^2} \right) + kA_{44} \left(\frac{\partial \Psi_y}{\partial y} + \frac{\partial^2 w}{\partial y^2} \right) + q(x, y, t) = \rho h \frac{\partial^2 w}{\partial t^2} \qquad (56)$$

Here w is the plate deflection, ρ is the laminate density, h is the laminate thickness, t is time, $q(x,y,t)$ the load, and ψ_x and ψ_y the shear rotations. The plate stiffness components D_{ij} and A_{ij} are determined using the FSDT [9]. The shear correction factor k is usually taken to be $\pi^2/12$ [3]. When assuming simply supported boundary conditions one can assume solutions for ψ_x, ψ_y, w, and q that satisfy these boundary conditions, for instance in the form of Equation 4. However, generally the rotary inertia (ψ_x and   ) are neglected. After substituting Equation 4 in Equation 56 and some transformation Equation 6 is obtained. The natural frequencies are given by Equation 57 [3].

$$\omega_{mn}^2 = \frac{C_{13} K_A + C_{23} K_B + C_{33}}{\rho h} \qquad (57)$$

where,

$$K_A = \frac{C_{12} C_{23} - C_{13} C_{22}}{C_{11} C_{22} - C_{12}^2} \qquad (58)$$

$$K_B = \frac{C_{12} C_{23} - C_{11} C_{23}}{C_{11} C_{22} - C_{12}^2} \qquad (59)$$

$$C_{11} = D_{11} \left(\frac{m\pi}{a} \right)^2 + D_{66} \left(\frac{n\pi}{b} \right)^2 + kA_{55} \qquad (60)$$

$$C_{12} = (D_{12} + D_{66}) \left(\frac{m\pi}{a} \right) \left(\frac{n\pi}{b} \right) \qquad (61)$$

$$C_{13} = kA_{55} \left(\frac{m\pi}{a} \right) \qquad (62)$$

$$C_{22} = D_{66} \left(\frac{m\pi}{a} \right)^2 + D_{22} \left(\frac{n\pi}{b} \right)^2 + kA_{44} \qquad (63)$$

$$C_{23} = kA_{44} \left(\frac{n\pi}{b} \right) \qquad (64)$$

$$C_{33} = kA_{55} \left(\frac{m\pi}{a} \right)^2 + kA_{44} \left(\frac{n\pi}{b} \right)^2 \qquad (65)$$

This page is intentionally left blank.